Available online at www.sciencedirect.com
SCIENCE DIRECT®
Journal of Sound and Vibration 271 (2004) 999–1014
JOURNAL OF SOUND AND VIBRATION
www.elsevier.com/locate/jsvi

Natural frequencies and damping estimation using wavelet transform of a frequency response function

H.P. Yin*, D. Duhamel, P. Argoul

Ecole Nationale des Ponts et Chaussées, LAMI ENPC-LCPC, 6 et 8 Avenue Blaise Pascal, Cité Descartes, Champs-sur-Marne, Marne-La-Vallée Cedex 2 77455, France

Received 3 October 2001; accepted 13 March 2003

Abstract

This paper deals with a general wavelet transform of FRFs for linear systems. Complex fractional functions are used as wavelets and properties of the wavelet transform are studied. Then an efficient method for estimating natural frequencies and dampings is proposed. The efficiency of the method is illustrated with both analytical and experimental data of frequency response functions.

1. Introduction

Vibrations are often regarded as unpleasant and unwanted phenomena causing such undesirable consequences as discomfort, noise, malfunctioning, wear, fatigue and even destruction. Modal analysis is one of the strong and reliable vibration analysis tools needed by modern engineering. Experimental modal analysis is the process of determining the modal parameters by way of an experimental approach. The modal parameters may be determined by analytical means, such as a finite element analysis, and one of the common reasons for experimental modal analysis is the verification/correction of the results of the analytical approach. Often, though, an analytical model does not always exist and the modal parameters determined experimentally serve as the model for future evaluations such as structural modifications.

Single-degree-of-freedom (s.d.o.f.) methods such as the power bandwidth method, the circle fit method [1,2] and the two-point finite difference formulae [3] are classical methods for modal parameter estimation. Recently, Yin and Duhamel [4] proposed a three-point finite difference formula; the application to both analytical data and experimental data has shown better accuracy

*Corresponding author. Tel.: 33-1-641-53-725; fax: 33-1-641-53-741.
E-mail address: yin@lami.enpc.fr (H.P. Yin).

0022-460X/$ - see front matter
doi:10.1016/j.jsv.2003.03.002

of the three-point finite difference formula compared to the two-point finite difference formula. Over the last 25 years, many multi-degree-of-freedom (m.d.o.f.) methods such as the least-squares complex exponential, the polyreference time domain, Ibrahim time domain, eigensystem realization algorithm, rational fraction polynomial, polyreference frequency domain and complex mode indicator function have been investigated. In the frequency domain, these methods generally use a least-squares method to select the modal parameters that minimize the difference between the measured frequency response function (FRF) and the function found by summing the contribution from the individual modes. These methods have been summarized in the books of Allemang [3], Maia et al. [5] and Heylen et al. [6]. M.d.o.f. methods are more accurate for structures with closely spaced modes, particularly when heavily damped. However, s.d.o.f. methods are quick, rarely involving much mathematical manipulation of the data, and give sufficiently accurate results of modal parameters for structures with well-separated modes. As indicated at the end of Section 4, the modal parameter estimation method presented is this paper which is based on the wavelet transform of FRFs should be considered as a s.d.o.f. method.

The methods of modal parameters estimation which are based on the integral transform analysis of dynamic responses of systems can be classified in two categories: some of these methods consider time responses such as impulse response functions, see for instance Refs. [7–9], while others analyze frequency responses which are most commonly FRFs [10,11]. Recently Yin and Argoul [12] introduced the wavelet transform of the FRFs using Cauchy's wavelet to estimate modal parameters. Applications to both analytical data and experimental data have shown the efficiency of this method [12,13]. In this paper, some theoretical generalizations and numerical convergence studies of this method are presented.

First, the analytical expression for wavelet transforms of FRFs, using a complex analytic function as a wavelet, is established. This analytical expression would be useful for the selection of appropriate wavelets for the analysis of FRFs. Then complex fractional functions are used as wavelets, because of their similarity to FRFs. The property of the wavelet transform of FRFs with this wavelet will be studied and a method for estimating the dampings and natural frequencies will be proposed. Finally, the method will be applied to both analytical and experimental data of FRFs in order to evaluate the accuracy of the method.

2. Brief presentation of the continuous wavelet transform

The continuous wavelet transform is presented briefly here. More information about this integral transform can be found in many books [14–16].

The continuous wavelet transform of a function $f(y)$ is defined as follows

$$W(a,b) = \frac{1}{\sqrt{a}} \int_{-\infty}^{+\infty} f(y)\phi^*\left(\frac{y-b}{a}\right) \mathrm{d}y, \tag{1}$$

where b and a are, respectively, position and scale variables. The scale variable a is positive. The signal to be analyzed is $f(y)$ and $\phi^*(x)$ is the conjugate of $\phi(x)$, the transforming function called the mother wavelet which serves as a prototype for generating the other window

functions (wavelets)

$$\phi_{a,b}(y) = \frac{1}{\sqrt{a}}\phi\left(\frac{y-b}{a}\right). \tag{2}$$

The continuous wavelet transform can be defined as the inner product of the signal to be analyzed with wavelets

$$W(a,b) = \int_{-\infty}^{+\infty} f(y)\phi^*_{a,b}(y)\,\mathrm{d}y. \tag{3}$$

In general, $\phi(x)$ must oscillate around zero and his magnitude must decay sufficiently fast when the value of x increases.

The wavelet transform can be seen as a measure of similarity between the wavelet and the signal to be analyzed. If the signal has a major component of frequency corresponding to the current scale, then the wavelet at the current scale will be similar or close to the signal at the particular location where this frequency component occurs. Therefore, the continuous wavelet transform will give a large value at this location and this scale. This feature of wavelet transform is essential for the understanding of the method proposed in this paper for the natural frequencies and dampings estimation.

3. Wavelet transform of FRFs

For systems whose motions are described by differential equations with constant coefficients, the FRFs are rational and can be written as a ratio of two polynomials in $\mathrm{j}\omega$

$$H(\omega) = \frac{\sum_{r=0}^{2N-1} a_r(\mathrm{j}\omega)^r}{\sum_{r=0}^{2N} b_r(\mathrm{j}\omega)^r}, \tag{4}$$

or as a sum of partial fraction functions

$$H(\omega) = \sum_{r=1}^{N}\left[\frac{A_r}{\mathrm{j}\omega-\lambda_r} + \frac{A_r^*}{\mathrm{j}\omega-\lambda_r^*}\right], \tag{5}$$

where N is the number of degrees of freedom, and $\lambda_r = \sigma_r + \mathrm{j}\omega_r$ is the rth complex pole, $\sigma_r < 0$, $\mathrm{j} = \sqrt{-1}$, A_r is the rth residue, λ_r^* and A_r^* are the conjugates of λ_r and A_r, respectively.

The continuous wavelet transform of the FRF is defined by

$$W(a,b) = \frac{1}{\sqrt{a}}\int_{-\infty}^{+\infty} H(\omega)\phi^*\left(\frac{\omega-b}{a}\right)\mathrm{d}\omega. \tag{6}$$

In order to simplify the presentation, let ψ denote the conjugate of ϕ, that is

$$\psi\left(\frac{\omega-b}{a}\right) = \phi^*\left(\frac{\omega-b}{a}\right). \tag{7}$$

Taking Eq. (5) into consideration, Eq. (6) becomes

$$W(a,b)=\frac{-\mathrm{j}}{\sqrt{a}}\left[\sum_{r=1}^{N}\left(A_r\int_{-\infty}^{+\infty}\frac{\psi((\omega-b)/a)}{(\omega+\mathrm{j}\lambda_r)}\,\mathrm{d}\omega+A_r^*\int_{-\infty}^{+\infty}\frac{\psi((\omega-b)/a)}{(\omega+\mathrm{j}\lambda_r^*)}\,\mathrm{d}\omega\right)\right]. \tag{8}$$

The integrals in the last equation can be evaluated, as in Ref. [10], by considering the following curvilinear integral in the complex plan

$$\oint\frac{\psi((s-b)/a)}{(s+\mathrm{j}\lambda_r)}\,\mathrm{d}s=\int_{-R}^{+R}\frac{\psi((s-b)/a)}{(s+\mathrm{j}\lambda_r)}\,\mathrm{d}s+\int_{HC}\frac{\psi((s-b)/a)}{(s+\mathrm{j}\lambda_r)}\,\mathrm{d}s. \tag{9}$$

The integration paths are shown by the right graph in Fig. 1. For the second integral and the third integral, they are, respectively, the straight line oriented from $s=(-R,0)$ to $s=(+R,0)$ and the half circle HC oriented from $s=(+R,0)$ to $s=(-R,0)$. The close path of the first integral is composed of the straight line and the half circle.

According to Cauchy's integral formula, any complex analytic function at any point in a zone can be represented using the values of this function on the boundary that delimits this zone

$$f(z)=\frac{1}{2\pi\mathrm{j}}\int_{\Gamma}\frac{f(s)}{(s-z)}\,\mathrm{d}s. \tag{10}$$

From this formula and provided that $\psi((s-b)/a)$ is analytic inside the half disc, the first integral in Eq. (8) is just the value of $2\pi\mathrm{j}\psi((s-b)/a)$ with s taken to be $-\mathrm{j}\lambda_r$

$$\oint\frac{\psi((s-b)/a)}{(s+\mathrm{j}\lambda_r)}\,\mathrm{d}s=2\pi\mathrm{j}\psi\left(\frac{-\mathrm{j}\lambda_r-b}{a}\right). \tag{11}$$

Because the magnitude of ψ tends sufficiently fast to zero, the last integral over the half circle in Eq. (9) will tend to zero when R becomes infinite

$$\int_{HC}\frac{\psi((s-b)/a)}{(s+\mathrm{j}\lambda_r)}\,\mathrm{d}s\to 0\quad\text{when}\quad R\to\infty. \tag{12}$$

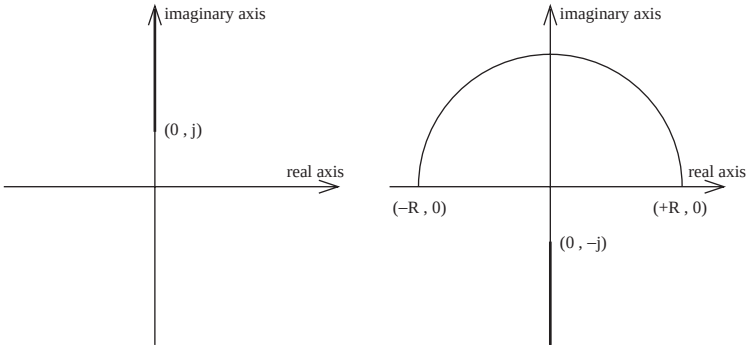

Fig. 1. The complex function $\phi_x(s)=(1+\mathrm{j}s)^{-(x+1)}$ is defined and analytic in the whole complex plane except on the superior part of imaginary axis above the point $(0,\mathrm{j})$ as shown by the left graph, its conjugate $\psi_x(s)=(1-\mathrm{j}s)^{-(x+1)}$ is defined and analytic in the whole complex plane except on the inferior part of imaginary axis under the point $(0,-\mathrm{j})$ as shown by the right graph.

From Eqs. (11) and (12), it can be deduced that

$$\int_{-\infty}^{+\infty} \frac{\psi((\omega-b)/a)}{(\omega+\mathrm{j}\lambda_r)}\,\mathrm{d}\omega = 2\pi\mathrm{j}\psi\left(\frac{-\mathrm{j}\lambda_r-b}{a}\right). \tag{13}$$

In a similar way, one can obtain

$$\int_{-\infty}^{+\infty} \frac{\psi((\omega-b)/a)}{(\omega+\mathrm{j}\lambda_r^*)}\,\mathrm{d}\omega = 2\pi\mathrm{j}\psi\left(\frac{-\mathrm{j}\lambda_r^*-b}{a}\right). \tag{14}$$

From the last two equations, the following result is established:

$$W(a,b) = \frac{2\pi}{\sqrt{a}}\sum\nolimits_{r=1}^{N}\left[A_r\psi\left(\frac{-\mathrm{j}\lambda_r-b}{a}\right) + A_r^*\psi\left(\frac{-\mathrm{j}\lambda_r^*-b}{a}\right)\right]. \tag{15}$$

This is a rather general result for wavelet transform of the FRFs. To construct a method for estimating natural frequencies and damping ratios, complex fractional functions will be used as wavelets in the next section.

4. Use of complex fractional functions as wavelet

Considering a complex variable s and the following complex fractional function

$$\phi_x(s) = \frac{1}{(1+\mathrm{j}s)^{x+1}} = \mathrm{e}^{-(x+1)\log(1+\mathrm{j}s)}, \tag{16}$$

where x is a positive real number. The complex logarithm $\log(z)$ is defined and analytic in the whole complex plane with a "slit" which is the negative real axis. So $\phi_x(s)$ is defined and analytic in the whole complex plane with a "slit" which is the semi-infinite vertical line above the point $s=(0,\mathrm{j})$, as shown by the left graph in Fig. 1.

The complex function $\psi_x(s)$, conjugate of $\phi_x(s)$

$$\psi_x(s) = \phi_x^*(s) = \frac{1}{(1-\mathrm{j}s)^{x+1}} = \mathrm{e}^{-(x+1)\log(1-\mathrm{j}s)} \tag{17}$$

is defined and analytic in the whole complex plane with a "slit" which is the semi-infinite vertical line under the point $s=(0,-\mathrm{j})$, as the right graph in Fig. 1 shows. When x is an integer number, $\phi_x(s)$ is the Cauchy's wavelet.

It can be verified that, for $x>0$, the complex fractional function wavelet $\phi_x(s)$ satisfies the admissibility condition. The real and imaginary parts of $\phi_x(s)$ for $x=1, 2.5, 4.5, 8$ are presented in Fig. 2.

Considering the continuous wavelet transform of the FRF and multiplying the transformed function by $(\sqrt{a})^{-x}$

$$H_x(a,b) = a^{-(x+1)/2}\int_{-\infty}^{+\infty} H(\omega)\phi_x^*\left(\frac{\omega-b}{a}\right)\mathrm{d}\omega. \tag{18}$$

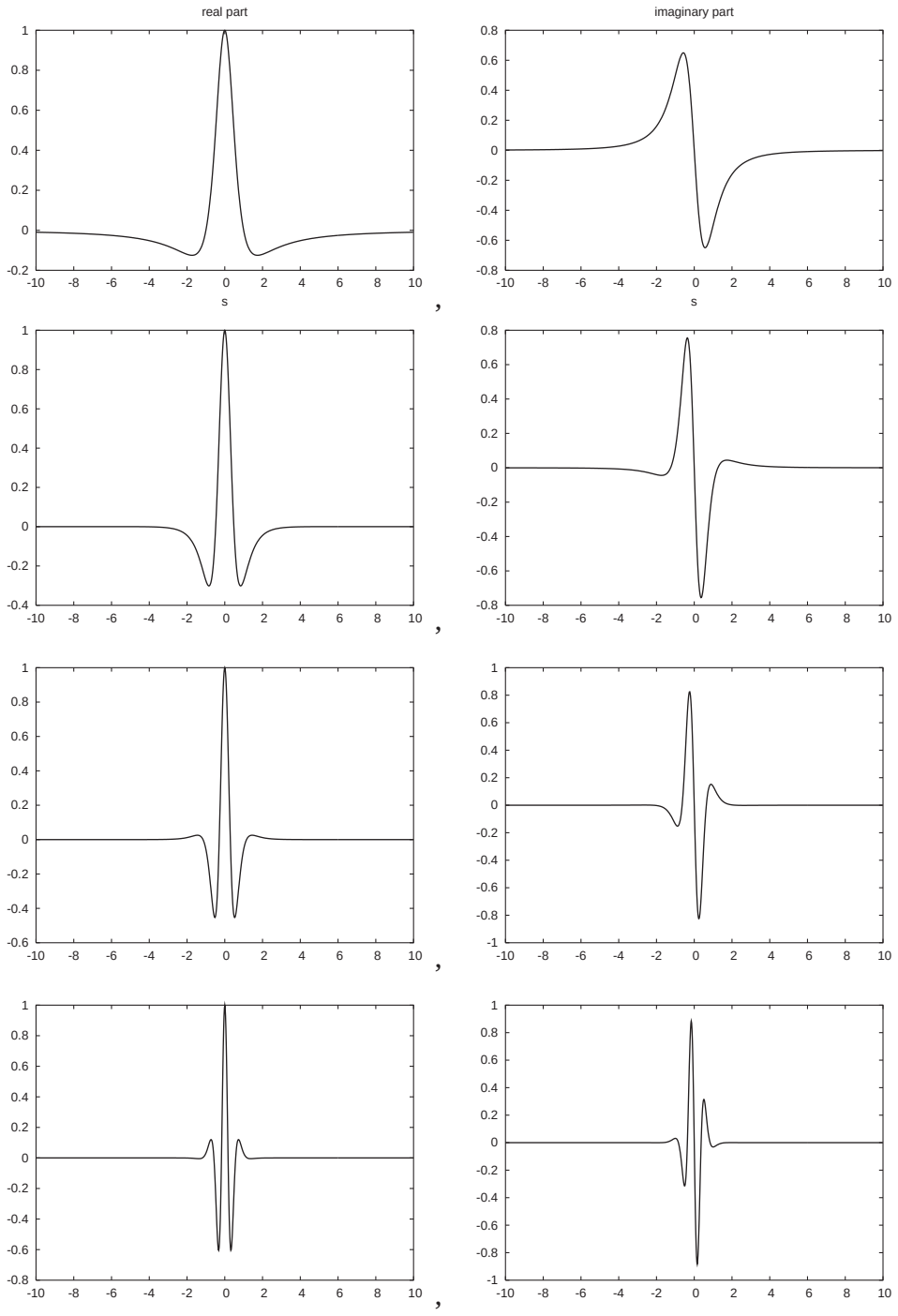

Fig. 2. Real part (left column) and imaginary part (right column) of the complex fractional function wavelets $\phi_x(s)$ for $x = 1$, 2.5, 4.5 and 8.

Since ψ_x is the conjugate of ϕ_x, this can be written as follows

$$H_x(a,b) = a^{-(x+1)/2} \int_{-\infty}^{+\infty} H(\omega)\psi_x\left(\frac{\omega - b}{a}\right) \mathrm{d}\omega. \tag{19}$$

The function $\psi_x(s)$ is analytic in the half plane over the real axis, so is $\psi_x((\omega - b)/a)$ because a is positive. Then Eq. (15) applies

$$H_x(a,b) = 2\pi a^{(x+1)/2} \sum\nolimits_{r=1}^{N} \left(\frac{A_r}{(a + \mathrm{j}b - \lambda_r)^{x+1}} + \frac{A_r^*}{(a + \mathrm{j}b - \lambda_r^*)^{x+1}}\right). \tag{20}$$

Since $\lambda_r = \sigma_r + \mathrm{j}\omega_r$, the last equation can be written as

$$H_x(a,b) = 2\pi a^{(x+1)/2} \times \sum_{r=1}^{N} \left(\frac{A_r}{[a - \sigma_r + \mathrm{j}(b - \omega_r)]^{x+1}} + \frac{A_r^*}{[a - \sigma_r + \mathrm{j}(b + \omega_r)]^{x+1}}\right). \tag{21}$$

Remember that σ_r is negative and a positive. Therefore the function $H_x(a,b)$ is always regular. It will be shown that the modulus of $H_x(a,b)$ presents a local maximum in the vicinity of each point $(a,b) = (-\sigma_r, \omega_r)$. Note that $-\sigma_r$ is positive.

It will be supposed that in the vicinity of $(-\sigma_r, \omega_r)$, i.e., if

$$\frac{a + \sigma_r}{\sigma_r} \ll 1 \quad \text{and} \quad \frac{b - \omega_r}{\sigma_r} \ll 1, \tag{22}$$

the behaviour of $H_x(a,b)$ in Eq. (21) is dominated by one single partial fractional function

$$H_x(a,b) \approx \frac{2\pi a^{(x+1)/2} A_r}{[a - \sigma_r + \mathrm{j}(b - \omega_r)]^{x+1}}. \tag{23}$$

Then the power expansion of the modulus of the regular function $H_x(a,b)$ until second order in the vicinity of $(-\sigma_r, \omega_r)$ can be easily established

$$|H_x(a,b)| \approx \frac{\pi |A_r|}{2^x |\sigma_r|^{(x+1)/2}} \left[1 - \frac{x+1}{2}\left(\frac{a + \sigma_r}{2\sigma_r}\right)^2 - \frac{x+1}{2}\left(\frac{b - \omega_r}{2\sigma_r}\right)^2\right]. \tag{24}$$

The above equation means that, provided that Eq. (23) is a good approximation, the absolute value of $H_x(a,b)$ describes roughly a paraboloid surface of revolution the summit location of which is close to $(-\sigma_r, \omega_r)$. This property suggests that the values of σ_r and ω_r could be estimated by determining the local maximum location of $|H_x(a,b)|$, i.e., if $|H_x(a_m, b_m)|$ is a maximum, then

$$\sigma_r \approx -a_m, \quad \omega_r \approx b_m. \tag{25}$$

The values of a_m and b_m depend a priori on the real variable x. This dependence will be studied for analytical data of FRFs in Section 5 and experimental data of a FRF in Section 6. To evaluate the stablility and the accuracy of the estimation of both natural frequency and damping, an

estimation stablility indicator function defined by the following equation:

$$I(x) = \frac{\sqrt{[a_m(x+\delta) - a_m(x)]^2 + [b_m(x+\delta) - b_m(x)]^2}}{\delta\sqrt{a_m^2(x) + b_m^2(x)}} \tag{26}$$

will also be studied, $\delta > 0$ being a small increment of x ($\delta = 0.125$ in Sections 5 and 6).

Due to the approximate relationship (23), the modal parameter estimation method described in this section should be considered as a s.d.o.f. method in a classification. However, there is a small difference between this method and classical s.d.o.f. methods. When the modal parameters of a mode are under estimation, in classical s.d.o.f. methods, the contribution of other modes to the FRF is neglected or approximated, while in the method proposed in this paper, the contribution of other modes to the wavelet transform of the FRF is neglected, see Eq. (23). This difference could explain why this s.d.o.f. method is more accurate than other s.d.o.f. methods such as the finite difference formulas (see Section 6).

5. Application to analytical data

Two-degrees-of-freedom systems are considered. The natural frequencies and dampings have been estimated for a FRF with two well-separated modes and a FRF with two closely spaced modes. In the case of well-separated modes, the undamped natural frequencies are 100 and 150 Hz. In the case of closely spaced modes, they are 100 and 107 Hz. The damping ratio is 2.5% in both cases.

The dependence on x of the estimated natural the frequencies, damping ratios and the estimation stability indicator function $I(x)$ defined by Eq. (26) are shown by the curves in Figs. 3 and 4. The estimated values are normalized, i.e., they have been divided by the correspondent exact values. The estimation stability indicator function decreases and the estimation accuracy increases as x increases, i.e., the higher the value of x the better the estimate. The estimation stability indicator function decreases rapidly when the value of x is small. When the value of x is beyond 2 for well-separated modes and beyond 4 for poorly separated modes, the indicator function becomes stable and the estimation becomes accurate.

These results suggest that the estimation is accurate if the estimation stability indicator function is stable and its values are small.

6. Application to experimental data

Now the experimental data of the FRF of a simple structure is considered. This structure is built from three Plexiglas beams positioned along a cross. The beams have a thickness of 0.5 cm and a width of 2 cm. The upper beam and the lower beam are horizontally placed, parallel to each other and of a length of 15.4 cm. The beam in the middle is also horizontally placed but perpendicular to the two others and a little shorter with a length of 12.9 cm. A random excitation signal has been used. This random excitation comes from below by a shaker (BK 4810) and is transmitted to the structure through an impedance head (BK 8001) which allows measurement of

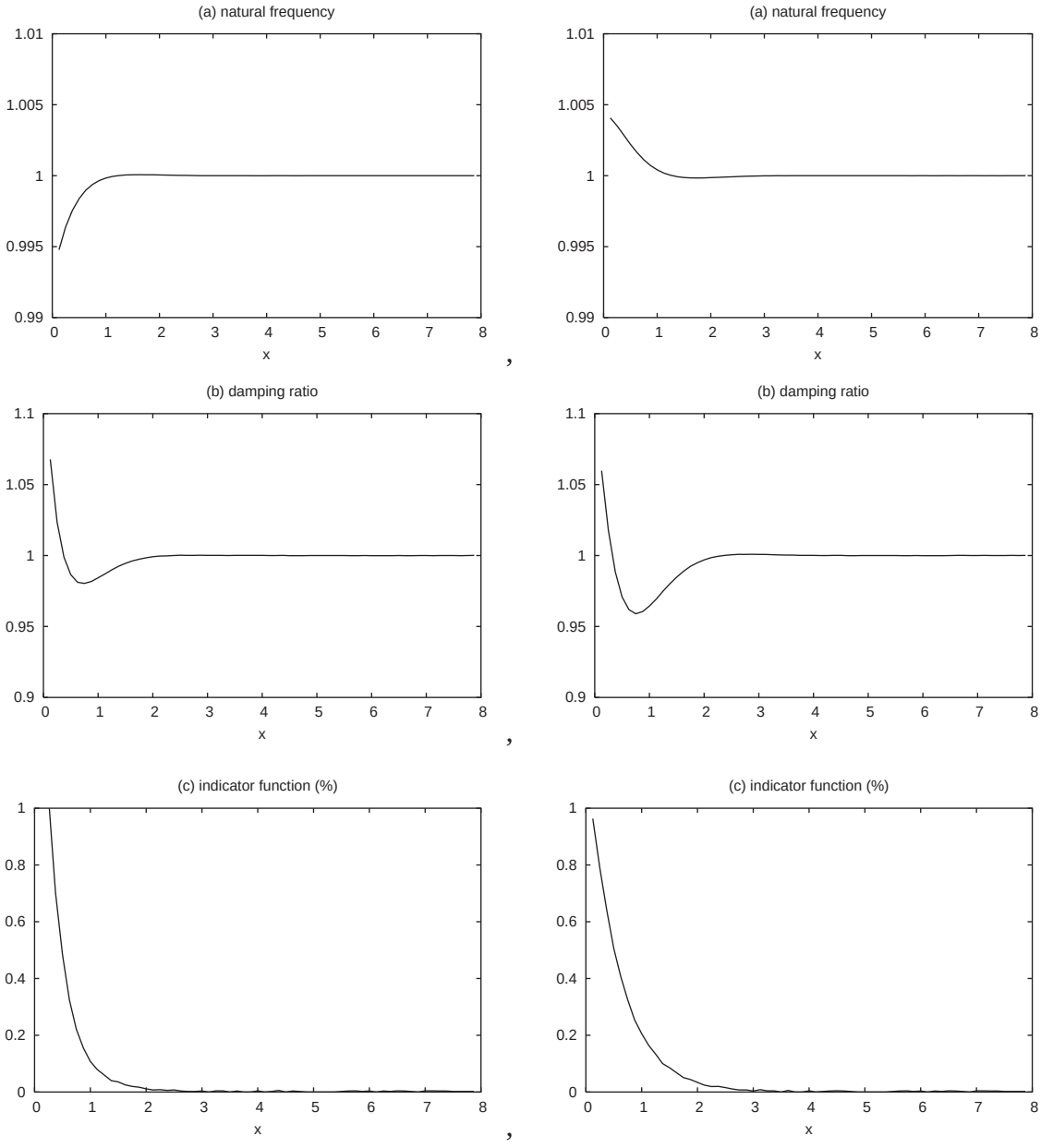

Fig. 3. Dependence on x of estimated natural frequency, damping and indicator function with two well-separated modes, left column for first mode and right column for second mode, the estimated values of natural frequency and damping are normalized by the exact values.

the acceleration and force just under the center of the structure. The acceleration is integrated twice to get the displacement and, the FRF between the displacement and the force is recorded by a signal analyzer (DI-PL202). The experimental data of the modulus of the FRF is presented in

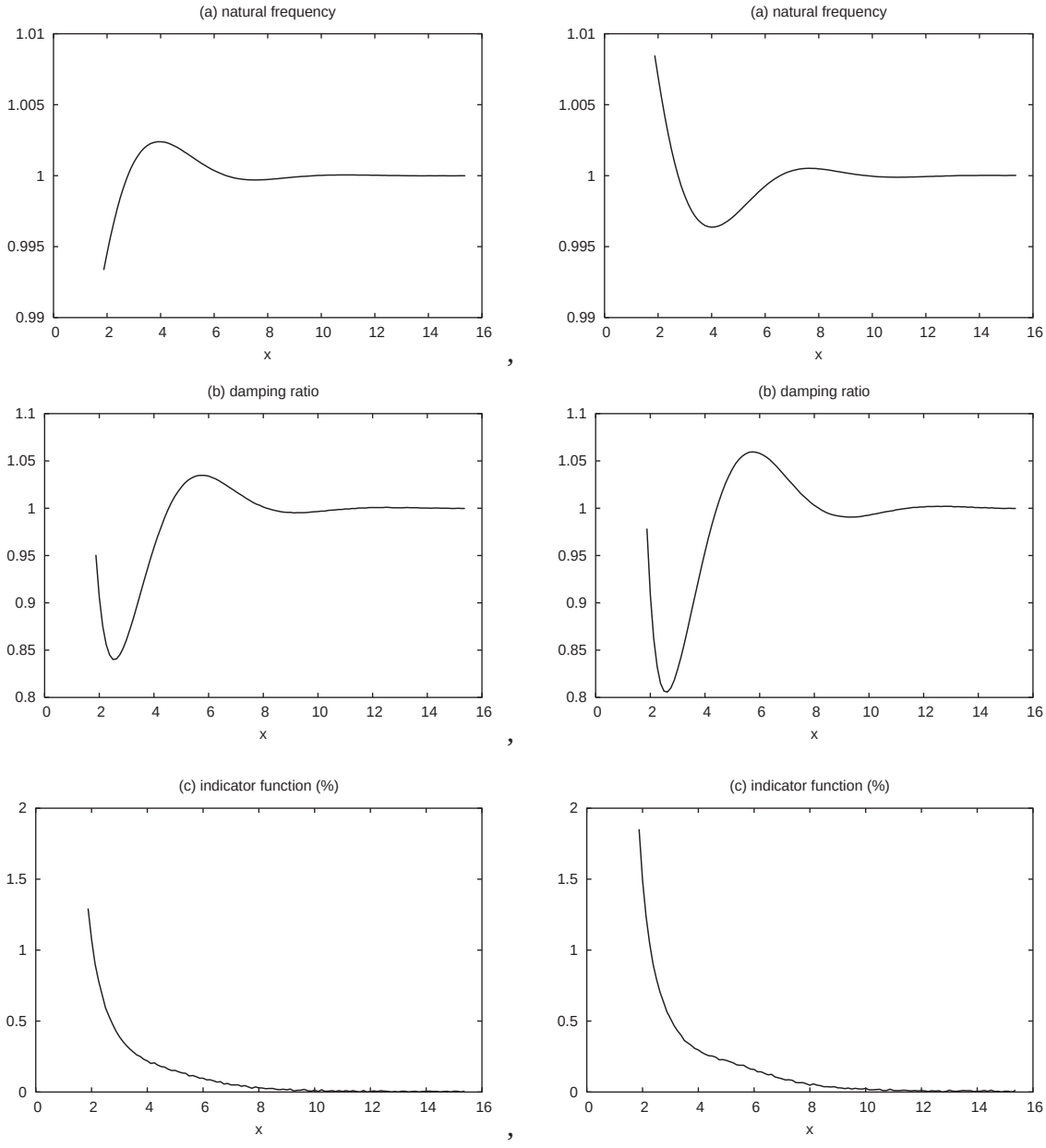

Fig. 4. Dependence on x of estimated natural frequency, damping and indicator function with two closely spaced modes, left column for first mode and right column for second mode, the estimated values of natural frequency and damping are normalized by the exact values.

Fig. 5. The FRF is normalized by the maximum value obtained near the first resonance. Three modes appear in the frequency range from 0 to 1000 Hz. The first two are coupled while the third is relatively isolated.

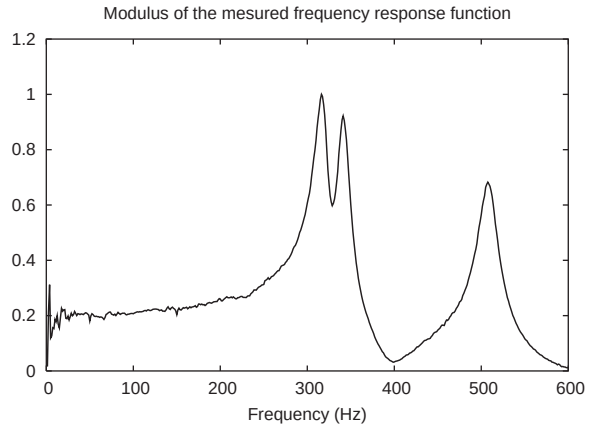

Fig. 5. Experimental data of FRF (modulus normalized by the maximum value near the first resonance).

To study the dependence of estimation on x, the value of x has been taken from 2 to 8. The integrals related to the wavelet transform of the FRF have been computed for different values of a and b. Local maxima of the modulus of $H_x(a,b)$ which is the wavelet transform of the FRF multiplied by $(\sqrt{a})^{-x}$ have been located. Then the values of b and a corresponding to theses maxima are used for estimating the natural frequencies and damping ratios, respectively.

The complex exponential method (a m.d.o.f. method) will be used as the reference method. Indeed, this method, although it appears to be sensitive to noise, is often used as a reference method [6]. By this method, the damped natural frequencies of the three modes are estimated to be 318.6, 341.1 and 508.4 Hz, and the damping ratios are estimated to be 2.56%, 2.32% and 2.23%.

The estimation results using the wavelet transform method described in Sections 3 and 4 for the three modes in the frequency range under consideration are presented in Figs. 6–8. Each value has been divided by that estimated by the complex exponential method. The estimation stability indicator function $I(x)$ is also presented.

For the third mode as shown in Fig. 8, the estimation stability indicator function decreases rapidly as x increases until 2. Then this function becomes stable and the estimation results too. But when x is greater than 6, they become unstable. For the first mode and the second mode as shown in Figs. 6 and 7, the estimation stability indicator function decreases rapidly as x increases until 4. Then this function becomes stable. But when x is beyond 5.5 for the first mode or beyond 6.875 for the second mode, the results become unstable. The deviation of the asymptotical behavior for the values of x beyond 5.5, 6.875 and 6 for respectively the first, second and third mode between the estimation results of the analytical data in Section 5 and those of the experimental data in this section, is probably due to the noise in the experimental data or the non-linear terms in the stiffness of the Plexiglas beams.

By comparing these results with those of analytical data in Section 5, it can be assumed that when the value of x is in an intermediate range where the estimation stability indicator function is stable and minimum, the estimation results are optimal. To involve a sufficient number of estimations in the calculation of the final average estimation, this intermediate range should be large enough. For our experimental data, this intermediate range should be $x \in [4, 5.5]$ in which

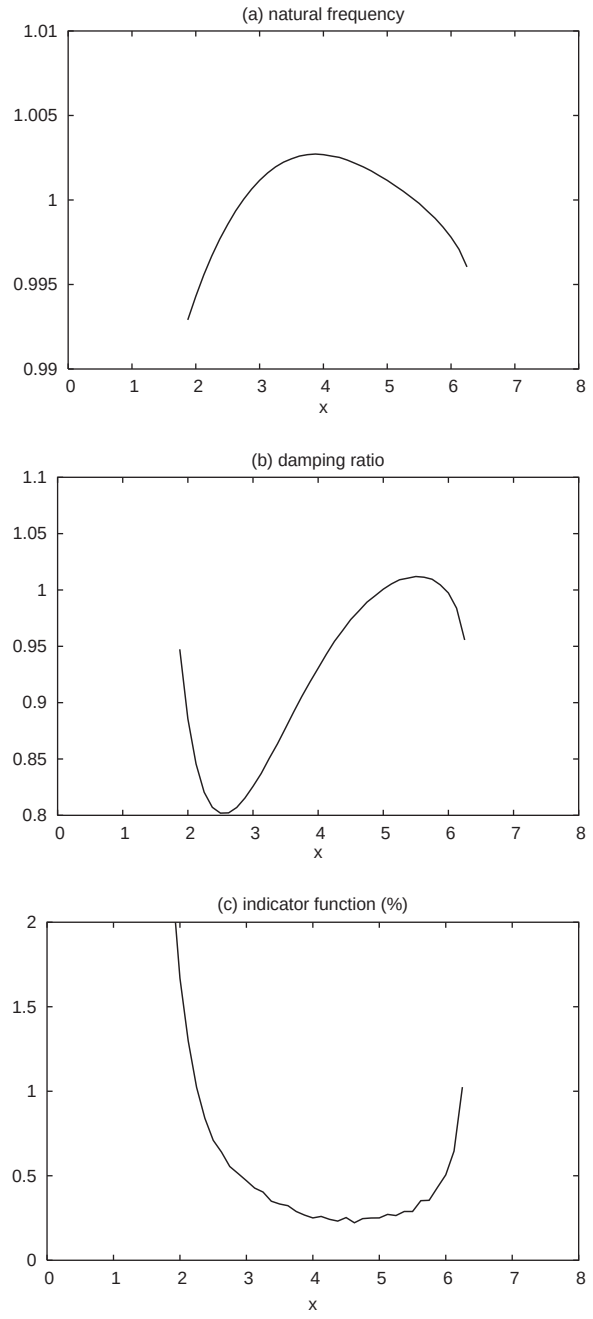

Fig. 6. Dependence on x of the estimated values of the natural frequency normalized by 318.6 Hz, the damping ratio normalized by 2.56% and the indicator function for the first mode. The reference values are estimated by the complex exponential method.

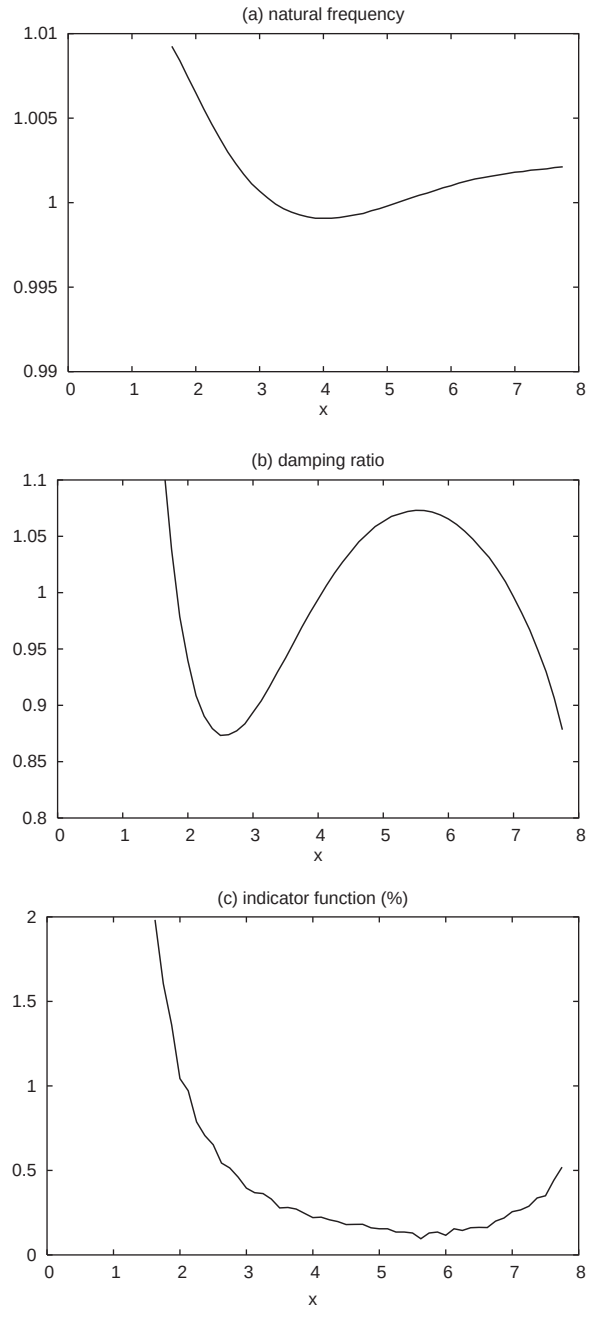

Fig. 7. Dependence on x of the estimated values of the natural frequency normalized by 341.1 Hz, the damping ratio normalized by 2.32% and the indicator function for the second mode. The reference values are estimated by the complex exponential method.

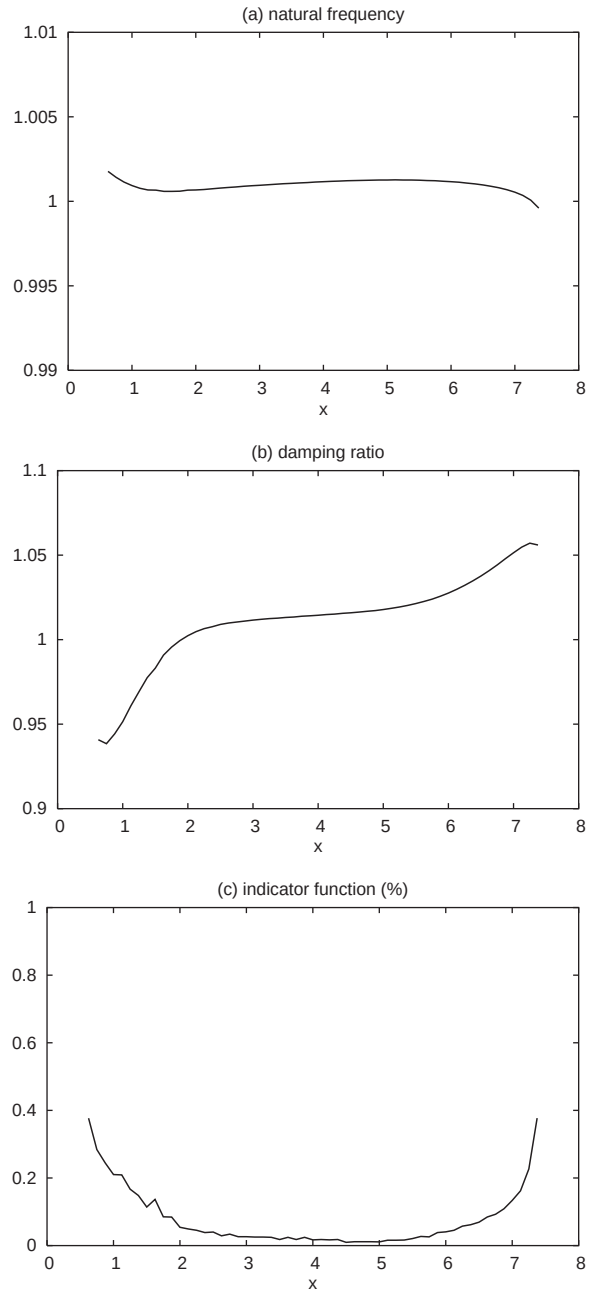

Fig. 8. Dependence on x of the estimated values of the natural frequency normalized by 508.4 Hz, the damping ratio normalized by 2.23% and the indicator function for the third mode. The reference values are estimated by the complex exponential method.

Table 1
Results of the natural frequencies and dampings of the three modes estimated by the method based on the wavelet transform of FRF, the three-point finite difference formula and the complex exponential method

	Mode number	1	2	3
FRF wavelet	Pole	$-50.4+2005.0$j	$-52.1+2143.9$j	$-72.4+3197.9$j
Transform method	Damping ratio	0.0252	0.0243	0.0226
Three-point finite	Pole	$-50.7+1994.0$j	$-45.2+2154.8$j	$-69.1+3195.2$j
Difference formula	Damping ratio	0.0254	0.0210	0.0216
Complex	Pole	$-51.2+2001.9$j	$-49.7+2143.2$j	$-71.3+3194.5$j
Exponential	Damping ratio	0.0256	0.0232	0.0223

$I(x)$ is stable and smaller than 0.3% for the first mode, $x\in[4, 6.875]$ in which $I(x)$ is stable and smaller than 0.25% for the second mode and $x\in[2, 6]$ in which $I(x)$ is stable and smaller than 0.05% for the third mode. The average estimation results of the natural frequencies and the dampings for the three modes have been computed in these ranges and are given in Table 1. Obviously, the estimation of the third mode is much better than that of the two coupled modes since $I(x)$ is much more stable and smaller for the third mode than for the two others. Compared to the estimation obtained from the very simple three-point finite difference formula, the estimation based on the wavelet transform of FRF is relatively close to the estimation obtained by using the complex exponential method, especially for the second mode.

7. Discussion and concluding remarks

The method for natural frequencies and dampings estimation proposed in this paper is based on the wavelet transform of frequency response functions (FRFs). The continuous wavelet transform of the FRF has been calculated analytically for any complex analytic function wavelets by using Cauchy's integral formula. When complex fractional functions are used as wavelets, the modulus of transformed function multiplied by $(\sqrt{a})^{-x}$ shows local maxima, x being a real variable for generating different mother wavalets. The natural frequencies and dampings can then be determined by searching the locations of these maxima.

Applications to both analytical and experimental data of FRFs have been made. The results have been compared to the exact values in the case of analytical data and to those estimated by the complex exponential method in the case of experimental data. The dependence on x of the estimation results has been studied. In the case of analytical data, the estimation accuracy always increases with the values of x, while in case of experimental data, the estimation accuracy increases rapidly when x is small and then become stable as in the case of analytical data, but diverge when x is beyond 5 or 6. The optimal estimation should be considered as the average results in an intermediate range of x where the estimation results are stable. Numerical results have shown that sufficiently accurate estimation for natural frequencies and damping ratios could be obtained with this method even if modes are not well separated.

The advantages of the method presented in this paper are the simplicity and the ability to give a quick estimation since only integrals need to be computed numerically. For closely spaced modes,

this method is not as accurate as m.d.o.f. methods. However, m.d.o.f. methods are time consuming and involve difficult numerical tasks and much mathematical manipulation of the data. Furthermore, the use of different methods is important in order to validate estimated modal parameters by comparison. It is interesting for engineers to compare the estimation of m.d.o.f. methods with a quick and sufficiently accurate estimation of a s.d.o.f. method. Besides, if accurate estimation is required, one can improve, via an iterative procedure, the accuracy of the presented method like other s.d.o.f. methods by subtracting the effect of modes already analyzed before analyzing the one of interest.

References

[1] C.C. Kennedy, C.D.P. Pancu, Use of vectors in vibration measurement and analysis, *Journal of Aeronautical Sciences* 14 (11) (1947) 603–625.
[2] D.J. Ewins, *Modal Testing: Theory and practice*, Research Studies Press, Ltd., Taunton, 1984.
[3] R.J. Allemang, *Vibration*: *Experimental Modal Analysis*, UC-SDRL-CN-20-263-662, 1995.
[4] H.P. Yin, D. Duhamel, Finite difference formulation for modal parameter estimation, *Journal of Sound and Vibration* 231 (2000) 259–275.
[5] N.M.M. Maia, J.M.M. Silva, J. He, N.A.J. Lieven, R.M. Lin, G.W. Skingle, W.M. To, A.P.V. Urgueira, *Theoretical and Experimental Modal Analysis*, Research Studies Press, Ltd., Taunton, 1996.
[6] W. Heylen, S. Lammens, P. Sas, *Modal Analysis Theory and Testing*, Katholieke Universiteit Leuven, Leuven, 1997.
[7] W.J. Staszewski, Identification of damping in M.d.o.f. systems using time-scale decomposition, *Journal of Sound and Vibration* 203 (1997) 283–305.
[8] M. Ruzzene, A. Fasana, L. Garibaldi, B. Piombo, Identification of damping in M.d.o.f. systems using time-scale decomposition, *Mechanical Systems and Signal Processing* 11 (1998) 207–218.
[9] A.N. Robertson, K.C. Park, K.F. Alvin, Identification of structural dynamics models using wavelet-generated impulse response data, *Journal of Vibration and Acoustics* 120 (1998) 261–266.
[10] L. Jezequel, P. Argoul, A new integral transform for linear systems identification, *Journal of Sound and Vibration* 111 (1986) 261–278.
[11] P. Argoul, Linear dynamical identification: an integral transform seen as a complex wavelet transform, *Meccanica* 32 (1997) 215–222.
[12] H.P. Yin, P. Argoul, Transformations intégrales et identification modale, *Comptes Rendus de l'Académie des Sciences Paris, Série II-b* 327 (1999) 777–783.
[13] H.P. Yin, P. Argoul, B. Guillermin, A. Horchler, Une méthode d'identification modale utilisant la fonction d'analyse des singularités, *Proceedings*, *Colloque National en Calcul des Structures*, Giens, 1999, pp. 851–856.
[14] Ch.K. Chui, *An Introduction to Wavelets*, Wavelets Analysis and Its Applications, Vol. 1, Academic Press, Boston, 1992.
[15] Y. Meyer, *Wavelet: Algorithm and Applications*, SIAM, Philadelphia, PA, 1993.
[16] B. Torrésani, Wavelet: *Analyse continue par ondelettes*, INterEdition/CNRS Edition, Paris, 1995.